

Copper-Transfer Mechanism from the Human Chaperone Atox1 to a Metal-Binding Domain of Wilson Disease Protein

Agustina Rodriguez-Granillo,[†] Alejandro Crespo,^{‡,§} Dario A. Estrin,^{||} and Pernilla Wittung-Stafshede^{*,†,⊥}

Department of Biochemistry and Cell Biology, Rice University, Houston, Texas 77251, Department of Bioengineering, Rice University, Houston, Texas 77005, Current address: Chemistry Modeling and Informatics, Merck Research Laboratories, Rahway, NJ 07065., Departamento de Química Inorgánica, Analítica y Química-Física, Facultad de Ciencias Exactas y Naturales, Universidad de Buenos Aires, Ciudad Universitaria, Pab. 2, C1428EHA Buenos Aires, Argentina, and Department of Chemistry, Umeå University, 901 87 Umeå, Sweden

Received: November 25, 2009; Revised Manuscript Received: January 25, 2010

The molecular details of how copper (Cu) is transferred from the human Cu chaperone Atox1 to metal-binding domains (MBDs) of P_{1B}-type ATPases are still unclear. Here, we use a computational approach, employing quantum mechanics/molecular mechanics (QM/MM) methods, to shed light on the reaction mechanism [probable intermediates, Cu(I) coordination geometries, activation barriers, and energetics] of Cu(I) transfer from Atox1 to the fourth MBD of Wilson disease protein (WD4). Both Atox1 and WD4 have solvent-exposed metal-binding motifs with two Cys residues that coordinate Cu(I). After assessing the existence of all possible 2-, 3- and 4-coordinate Cu-intermediate species, one dominant reaction path emerged. First, without activation barrier, WD4's Cys1 binds Cu(I) in Atox1 to form a 3-coordinated intermediate. Next, with an activation barrier of about 9.5 kcal/mol, a second 3-coordinated intermediate forms that involves both of the Cys residues in WD4 and Cys1 of Atox1. This species can then form the product by decoordination of Atox1's Cys1 (barrier of about 8 kcal/mol). Overall, the Cu-transfer reaction from Atox1 to WD4 appears to be kinetically accessible but less energetically favorable ($\Delta E = 7.7$ kcal/mol). Our results provide unique insights into the molecular mechanism of protein-mediated Cu(I) transfer in the secretory pathway and are in agreement with existing experimental data.

Introduction

Intracellular copper (Cu) levels are tightly regulated, because, even though Cu is an essential trace metal found in the active sites of key enzymes, it can be toxic at high levels. Cells utilize highly conserved pathways to manage the uptake, storage, and export of Cu.^{1,2} These metal-homeostasis pathways require high protein–protein specificity, to avoid the mishandling of the metal and irreversible macromolecular oxidation, and generally involve a Cu chaperone that binds and delivers Cu to cellular targets. In the case of Cu transport to the secretory pathway, this specificity appears to arise from the fact that the metallochaperone and target domains share the same fold and metal-binding motif.

In humans, the Cu chaperone Atox1 (or HAH1) delivers Cu(I) to the metal-binding domains (MBDs) of two P_{1B}-type ATPases: the Menkes (ATP7A) and Wilson (ATP7B) disease proteins.^{3–5} Each ATPase has six soluble MBDs, which have been shown to interact differently with Atox1 in a metal-dependent manner.^{6–12} Both Atox1 and the MBDs bind one Cu(I) through two Cys residues located in a conserved MX₁C₁X₂X₃C₂ motif.^{13,14} Cu(I) transfer is believed to occur through an Atox1–Cu–MBD

adduct in which Cu(I) is transiently shared by the two proteins^{15–18} and might involve 2-, 3- and/or 4-coordinate Cu intermediates^{17,19,20} (Table 1). However, the mechanism, thermodynamics, and kinetics of this reaction are unknown. In this work, we investigated the reaction pathway of Cu(I) transfer from holo-Atox1 to the fourth MBD in ATP7B (WD4) using quantum mechanics/molecular mechanics (QM/MM) calculations (Figure 1). Although Atox1 selectively transfers Cu(I) to both WD2 and WD4 in vivo, WD4 was chosen as the target domain because there is a PDB-reported structure only for WD4¹¹ and also because WD4 is the strongest Atox1 binder in vitro¹⁰ and in silico.²¹ Upon probing all different possible reaction pathways, we found that 3-coordinated intermediates, in which Cu(I) is shared by either of the Cys1 residues from both proteins, are more stable than 2- or 4-coordinated intermediates. Also, it emerged that, whereas the Cu(I)-transfer reaction from Atox1 to WD4 is kinetically feasible, it is less energetically favorable.

Computational Methods

Initial Structures for Molecular Dynamics Simulations.

The initial structure for the reactant heterocomplex was taken from our previously generated holo-Atox1–WD4 heterocomplex structure,²¹ which consists of apo-WD4 (2ROP¹¹) and the final structure of holo-Atox1 obtained after molecular dynamics (MD) simulations.²² The initial structure for the product heterocomplex (consisting of apo-Atox1 and holo-WD4) is the same as the reactant structure, except that the Cu(I) atom coordinates the two Cys residues in WD4. At the time we started this analysis,

* To whom correspondence should be addressed. E-mail: pernilla.wittung@chem.umu.se.

[†] Department of Biochemistry and Cell Biology, Rice University.

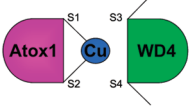
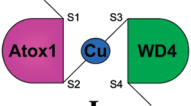

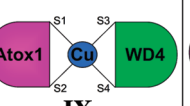
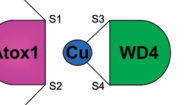
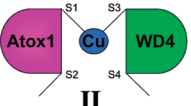

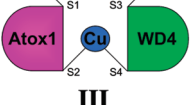

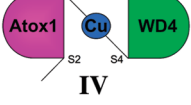

[‡] Department of Bioengineering, Rice University.

[§] Current address: Chemistry Modeling and Informatics, Merck Research Laboratories, Rahway, NJ 07065.

^{||} Universidad de Buenos Aires.

[⊥] Umeå University.

TABLE 1: List of Reactant, Product and All Possible Intermediates in the Cu-Transfer Reaction from holo-Atox1 to apo-WD4, Indicating the Corresponding Cu(I) Center Geometry^a

reactant	2-coordinated intermediates	3-coordinated intermediates	4-coordinated intermediate	product
	 I	 V	 IX	
	 II	 VI		
	 III	 VII		
	 IV	 VIII		

^a S1 and S2, Atox1's Cys1(SG) and Cys2(SG), respectively; S3 and S4, WD4's Cys1(SG) and Cys2(SG), respectively.

the structure of Atox1–Cu–MK1 was not available.¹⁷ Therefore, the relative orientation of the proteins in the Atox1–WD4 heterocomplex was obtained by homology threading calculations²³ using the holo-Atox1 homodimer crystal structure (1FEE) as a reference.¹⁹ Based on NMR data, including the recently published Atox1–Cu–MK1 structure,^{10,11,17,24,25} the contact regions in our heterocomplexes match the contact regions in the metallochaperone–target adduct.

MD Simulations. All simulations were performed using Amber 9^{26–29} as described in ref 21. The initial structures were immersed in a pre-equilibrated truncated octahedral cell of TIP3P explicit water molecules,³⁰ and counterions were added to neutralize the systems;²⁹ water molecules extended at least 10 Å from the surface of the proteins. The coordinating Cys and Cu(I) in the holo forms were parametrized as described in ref 22 for the reactant [Cu(I) coordinated to Atox1] and using the parameters developed in ref 21 for the product [Cu(I) coordinated to WD4]. The rest of the protein atoms were described with the parm99SB force-field parametrization.³¹ The protonation state of the titratable residues corresponds to the stable form at pH 7. Simulations were performed in the *NPT* ensemble (constant pressure of 1 atm and temperature of 300 K) were maintained using the Berendsen coupling scheme³², employing periodic boundary conditions. The SHAKE algorithm was employed to keep bonds involving hydrogen atoms at their equilibrium lengths.³³ The systems were optimized and equilibrated for 200 ps at 300 K. The structures were then simulated until the root-mean-square deviation (rmsd) as a function of time was stable for at least 50 ns, although the total simulation time was ~120 ns for each. Values of rmsd and rms fluctuations (rmsf) per residue were calculated for each system using the ptraj module of Amber 9.^{26–29}

Free Energy Calculations. Atox1–WD4 binding free energies (ΔG) for both reactant and product heterocomplexes were estimated using the sietraj program.^{34,35} This program calculates ΔG for snapshot structures from the MD simulations as the sum

of the intermolecular van der Waals and Coulomb interactions plus the change in reaction field energy (determined by solving the Poisson–Boltzmann equation) and nonpolar solvation energy (proportional to the solvent-accessible surface area). ΔG is then scaled by an empirically determined factor based on binding affinities in solution.³⁴ The scaling can be considered a crude treatment of entropy–enthalpy compensation, but still contains the caveats of implicit solvation.^{34,36} Here, we estimated ΔG by averaging 500 calculations from the last 50 ns of the MD simulations of the two heterocomplexes.

Initial Structure for QM/MM Calculations. A snapshot from the MM/MD simulation of the reactant Atox1–WD4 heterocomplex, in which WD4's Cys residues were close to Atox1's active site [$d_{S-Cu(I)} < 5$ Å], was selected as the initial structure of the reactant. Starting from this structure, we simulated 1 ns of MD constraining WD4's Cys geometries by applying a harmonic constraint to both $S_{WD4}-Cu_{Atox1}$ distances (equilibrium distance of 3.5 Å) and to both of WD4's Cys dihedral angles along the axis of the CA–CB bond, so that SG pointed toward Atox1's Cu(I) atom. This was followed by a simulated annealing calculation (200 ps) in which the temperature was slowly decreased to 0 K, applying the same geometrical constraints. We then performed a free MM geometry optimization of the whole system, followed by a QM/MM optimization in which the Cu(I) atom plus the four methylthiolate groups of the Cys residues were treated as the QM subsystem (see simulation details below).

QM/MM Calculations. Simulations were performed with a QM/MM implementation³⁷ of the SIESTA code³⁸ in which the QM subsystem was treated at the density functional theory (DFT) level. For all atoms, basis sets of double- ξ plus polarization quality were employed, with a pseudoatomic orbital energy shift of 25 meV and a grid cutoff of 150 Ry.³⁸ All QM/MM calculations were performed using the PBE functional,³⁹ in the low-spin state. This combination of functional, basis set, and grid parameters was previously validated for the isolated

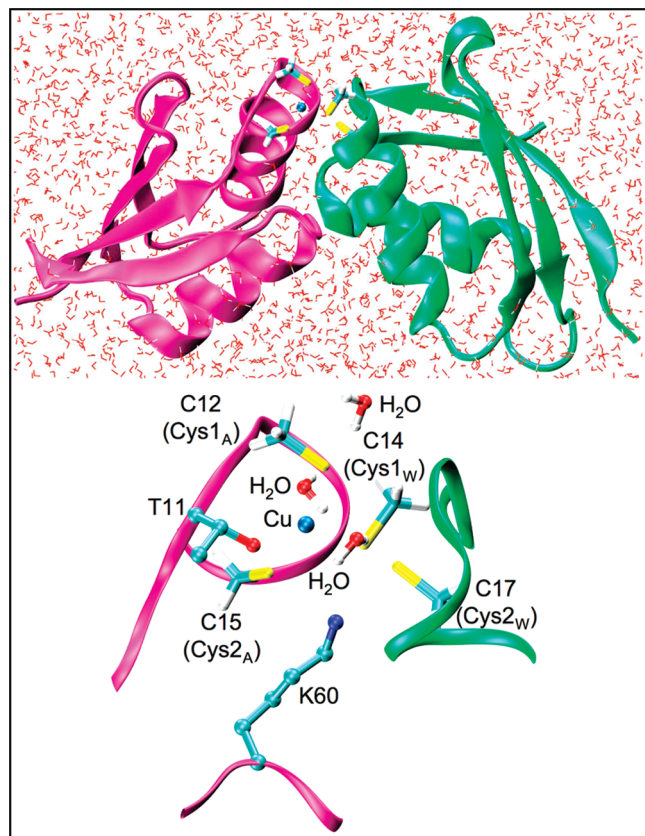


Figure 1. Top: QM/MM-optimized structure of the holo-Atox1-WD4 heterocomplex that involves the reactant (i.e., Cu-Atox1 and apo-WD4). The QM subsystem [Cu(I) plus four methylthiolate groups] is shown in licorice style; the rest of the system (protein plus solvent) corresponds to the MM subsystem. Bottom: Enlargement of holo-Atox1 and WD4 active sites. The QM subsystem is shown in licorice style, and relevant MM residues (Atox1's Thr11 and Lys60, plus three water molecules) are shown in CPK style. The sulfur atoms of Cys12 and Cys15 in Atox1 (Cys1_A and Cys2_A) and Cys14 and Cys17 in WD4 (Cys1_W and Cys2_W) are referred to as S1, S2, S3, and S4, respectively, in Tables 1, 2, and 4 and Figures 2–7 and S1–S9 (Supporting Information).

model systems²² $[\text{Cu}^+(\text{CH}_3\text{S}^-)_2]^-$ and $[\text{Cu}^+(\text{CH}_3\text{S}^-)_3]^-$ and in similar molecular systems that include Cu atoms.^{21,22,40}

To investigate the reaction mechanisms of Cu(I) transfer from holo-Atox1 to WD4, we performed QM/MM restrained energy optimizations along selected reaction coordinates (Table 2). For this purpose, an additional term is added to the potential energy according to the expression $V(\xi) = k(\xi - \xi_0)^2$, where k is an adjustable force constant, ξ is the value of the reaction coordinate in the system-particular configuration, and ξ_0 is the reference value of the reaction coordinate. By varying ξ_0 , the system is forced to follow the minimum reaction path along the given coordinate. In all cases, the force constant was 100 kcal/(mol Å²).

For reactions A–S, the Cu(I) atom plus the four methylthiolate groups of Atox1's Cys12 and Cys15 (Cys1_A and Cys2_A) and WD4's Cys14 and Cys17 (Cys1_W and Cys2_W) were selected as the QM subsystem, which comprises 21 atoms. For reactions A', B', and R' the Cu(I) atom, three methylthiolate groups, and one methylthiol group (Cys2_W, Cys1_W, and Cys2_A for reactions A', B', and R', respectively) were selected as the QM subsystem, comprising 22 atoms. The rest of the protein, counterions, and water molecules were treated classically. We allowed free motion for the QM atoms and for the MM atoms located inside a sphere of 12 Å from the QM subsystem center of mass. The

TABLE 2: Definition (ζ^a) and Initial (ζ_{initial}) and Final (ζ_{final}) Values^b of the Reaction Coordinate for Each Reaction A–S, A', B', and R' ^c

reaction	reaction coordinate (ζ)	ζ_{initial}	ζ_{final}
A	S3–Cu	3.5	2.3
B	S4–Cu	3.8	2.3
C	S4–Cu	3.8	2.3
	S3–Cu	3.5	3.5
D	(S2–Cu) – (S3–Cu)	0.7	–1.3
E	(S1–Cu) – (S3–Cu)	–1.4	1.4
F	(S2–Cu) – (S3–Cu)	–1.4	1.4
G	(S2–Cu) – (S4–Cu)	–1.6	1.4
H	(S1–Cu) – (S4–Cu)	–1.6	1.4
I	(S3–Cu) + (S4–Cu) – (S1–Cu)	5.1	0.8
J	(S3–Cu) + (S4–Cu) – (S2–Cu)	5.1	0.8
K	(S3–Cu) + (S4–Cu)	7.3	4.6
L	S1–Cu	2.3	3.6
M	S2–Cu	2.3	3.6
N	S4–Cu	3.6	2.3
O	(S1–Cu) – (S4–Cu)	–1.3	1.3
P	(S2–Cu) + (S4–Cu)	–1.3	1.3
Q	(S1–Cu) + (S2–Cu) – (S4–Cu)	1.0	5.0
R	S1–Cu	2.3	4.0
S	(S3–Cu) + (S4–Cu) – (S1–Cu) – (S2–Cu)	2.9	–2.8
A'	S3–Cu	3.5	2.3
B'	S4–Cu	3.7	2.3
R'	S1–Cu	2.3	3.7

^a ζ is always defined as a linear combination of the distance between Atox1's and WD4's Cys1(SG) and Cys2(SG) (S1–S4) and Cu(I). ^b Both values in Å. ^c S1 and S2, Atox1's Cys1(SG) and Cys2(SG), respectively; S3 and S4, WD4's Cys1(SG) and Cys2(SG), respectively.

frontier between the QM and MM portions of the system (Cys CA–CB bond) was treated by the SPLAM method.⁴¹ The MM subsystem was treated using the Amber99 force-field parameterization⁴² for protein and counterions atoms and TIP3P for water molecules.³⁰

Results and Discussion

Finding the First Intermediate. Starting from the optimized structure of holo-Atox1 and apo-WD4, the reactant (Figure 1), we first probed the energetics of binding either of WD4's Cys residues (reactions A and B, Table 2, Figure 2). Coordination of WD4's Cys1 (Cys1_W) occurs without activation energy (E_a), and this intermediate, **V**, is more energetically stable than the reactant (Table 3). Coordination of WD4's Cys2 (Cys2_W) occurs with a nonzero E_a (Table 3) and yields a different intermediate than expected: **VII** instead of **VI** (Table 1). This suggests that the 3-coordinate intermediate in which Cu(I) is coordinated by Cys1 from both proteins (**VII**) is more stable than the one in which only Cys1 from Atox1 (Cys1_A) coordinates Cu(I) (**VI**).

Because we wanted to assess the energetics of binding of Cys2_W, we performed two different reactions: (i) same as reaction B but fixing Cys1_W [reaction C, Table 2, Figure S1 (Supporting Information)], to avoid formation of intermediate **VII**, and (ii) starting from intermediate **VII** to obtain intermediate **VI** [reaction D, Table 2, Figure S1 (Supporting Information)]. Both reactions yield the desired intermediate **VI**, which has higher energy than the reactant (Table 3) and is not at a minimum in the potential energy surface (Figure S1, Supporting Information). From these reactions, it appears that Cys1_W will bind first to Cu-Atox1 to form a stable 3-coordinated intermediate (**V**). Binding of Cys2_W alone (without subsequent binding of Cys1_W) is not energetically or kinetically favorable.

To assess the possibility of a 2-coordinated species being the first intermediate of the Cu-transfer reaction, we performed reactions E–H (Table 2, Figure 3). None of these reactions

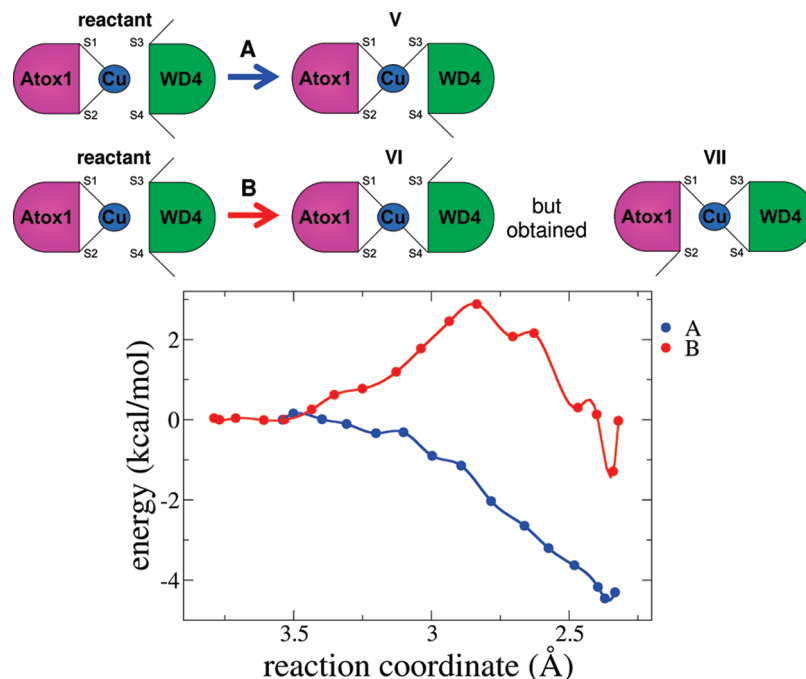


Figure 2. Potential energy profile (kcal/mol) along the corresponding reaction coordinate (Å) defined in Table 2 for reactions A (blue) and B (red). A schematic of the species (defined in Table 1) involved in each reaction is also shown.

TABLE 3: Activation Energy (E_a), Difference in Potential Energy (ΔE), and Type of Intermediate Found for Each Reaction A–S, A', B' and R', for the Corresponding First, Second, or Third Step

reaction	E_a (kcal/mol)			ΔE (kcal/mol)			intermediate-like	
	first	second	third	first	second	third	first	second
A	0	—	—	-4.5	—	—	—	—
B	2.9	—	—	-1.3	—	—	—	—
C	6.0	—	—	6.0	—	—	—	—
D	4.5	—	—	4.5	—	—	—	—
E	0	17.3	—	-4.2	17.3	—	V	—
F	0	10.8	—	-4.0	10.8	—	V	—
G	2.2	1.2	—	-1.4	1.2	—	VII	—
H	4.0	7.8	—	-2.3	7.8	—	VII	—
I	0	8.4	—	-1.5	8.4	—	V	—
J	1.3	8.9	—	-2.0	8.9	—	V	—
K	0	5.6	—	-2.9	5.6	—	V	—
L	17.5	—	—	17.5	—	—	—	—
M	12.6	—	—	12.6	—	—	—	—
N	7.5	—	—	7.5	—	—	—	—
O	11.5	3.8	—	9.6	3.0	—	VIII	—
P	9.5	—	—	6.4	—	—	—	—
Q	10.1	2.1	3.7	8.6	-0.8	2.1	VII	VII
R	8.1	—	—	5.8	—	—	—	—
S	2.8	5.3	7.1	-3.4	2.3	6.8	V	VII
A'	0	—	—	-3.5	—	—	—	—
B'	6.1	—	—	6.1	—	—	—	—
R'	10.2	—	—	4.2	—	—	—	—

occur in a concerted fashion; instead, they all proceed through formation of a 3-coordinated intermediate, which is always more stable than the product. This suggests that 2-coordinated intermediates are not likely to occur during the Cu(I)-transfer process from Atox1 to WD4. To form 2-coordinated species in which Cys1_W is bound to Cu(I), both reactions E and F start by binding Cys1_W to form the stable 3-coordinated intermediate V with no E_a (Table 3, Figure 3). Following formation of intermediate V, the reactions continue to obtain the 2-coordinated metastable species. In both cases, decoordination of either of Atox1's Cys residues occurs with a large kinetic barrier. However, species II is more stable than I, suggesting again that intermediates in which the Cys1 residues from both Atox1 and WD4 are bound to Cu(I) are the most stable. On the other hand,

neither reaction G nor reaction H yields the desired intermediate (Figure 3), suggesting that these two dicoordinated intermediates (III and IV) are not stable species in the Cu-transfer reaction and, therefore, are not likely to be populated in vivo or in vitro. Both reactions begin by coordination of both of WD4's Cys residues and decoordination of Atox1's Cys2 (Cys2_A), to form the stable 3-coordinated intermediate VII (Table 3, Figure 3). As in reaction B, this step occurs with $E_a \approx 2\text{--}4$ kcal/mol. In the case of G, the reaction continues to form a similar 3-coordinated intermediate VII, which only differs by ~ 1 kcal/mol. In the case of H, the reaction continues to form the final product of the global reaction, which is higher in energy by ~ 8 kcal/mol. Overall, based on reactions E–H, we propose that (i) 3-coordinated intermediates are more stable than 2-coordinate intermediates in the Cu-transfer reaction and (ii) the 3-coordinated intermediate V (more reactant-like) is more stable than the 3-coordinated intermediate VII (more product-like).

We next explored the possibility of obtaining the 3-coordinated intermediates VII or VIII as the first intermediates of the reaction [reactions I and J, Table 2, Figure S2 (Supporting Information)] starting from the reactant geometry. As for reactions E–H, both reactions I and J proceed in a nonconcerted way, starting by the initial binding of Cys1_W to form intermediate V, with no (reaction I) or small (reaction J) kinetic barrier (Table 3). However, as opposed to reaction J, reaction I does not yield the desired intermediate VIII, suggesting that intermediate VII and not VIII is likely an intermediate of the global Cu(I)-transfer reaction. In the case of reaction I, the reaction proceeds to form the final product of the global reaction, with a kinetic barrier of ~ 8 kcal/mol. On the other hand, in reaction J, the reaction continues from intermediate V to finally form species VII, after overcoming an energy barrier (E_a) of ~ 9 kcal/mol.

Next, we calculated the energy profile of forming the 4-coordinated species (intermediate IX), in which Cu(I) is coordinated by both Cys residues of Atox1 and WD4 (reaction K, Table 2, Figure 4). In agreement with all reactions above, the initial step involves binding of Cys1_W without a kinetic

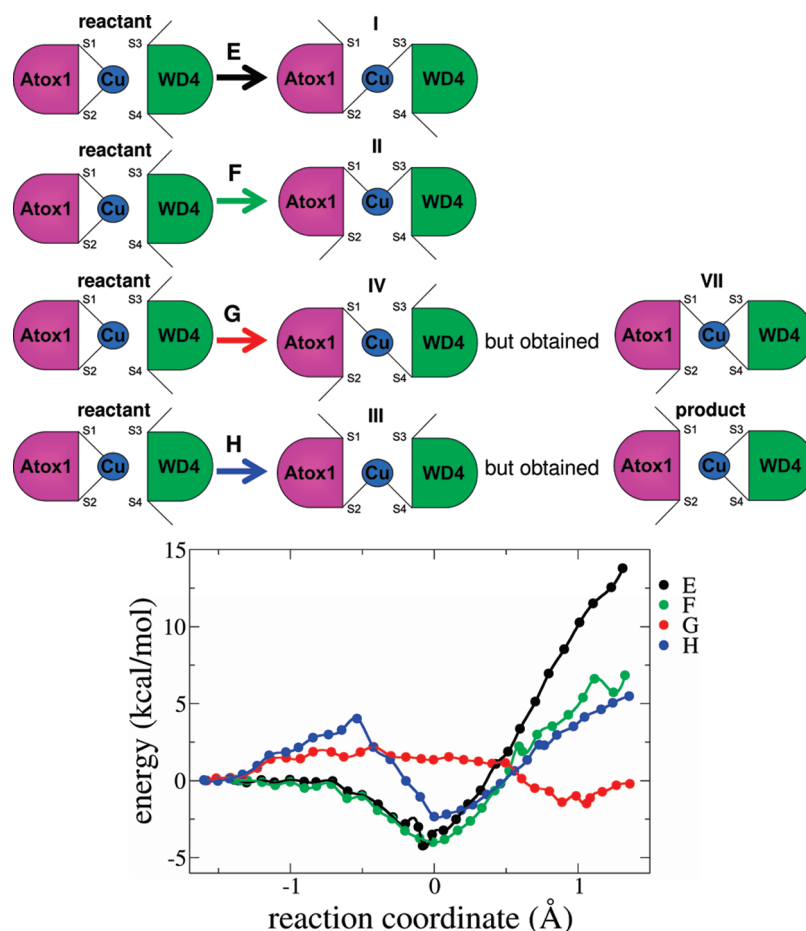


Figure 3. Potential energy profile (kcal/mol) along the corresponding reaction coordinate (Å) defined in Table 2 for reactions E (black), F (green), G (red), and H (blue). A schematic of the species (defined in Table 1) involved in each reaction is also shown.

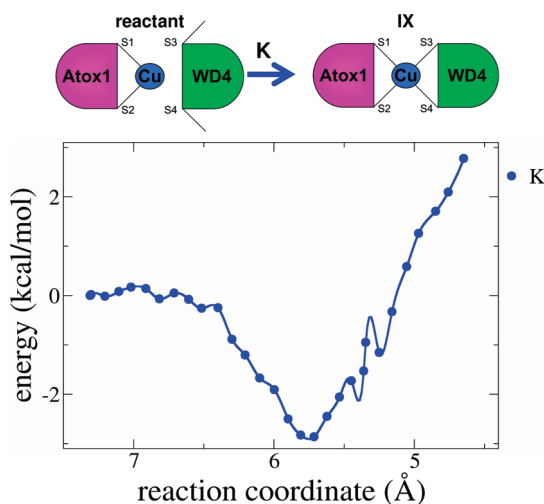


Figure 4. Potential energy profile (kcal/mol) along the corresponding reaction coordinate (Å) defined in Table 2 for reaction K. A schematic of the species (defined in Table 1) involved in the reaction is also shown.

barrier, to form intermediate **V** (Table 3). Finally, Cys2_W binds to form the metastable tetrahedral intermediate with $E_a \approx 6$ kcal/mol. Intermediate **IX** is not a minimum in the energy profile, suggesting that a tetrahedral species is not likely to be a probable intermediate in the Cu-transfer reaction between these proteins.

Overall, these calculations suggest that the initial step in the global Cu-transfer reaction from Atox1 to WD4 is coordination of Cys1_W to form 3-coordinated intermediate **V**. This reaction

occurs with no or small activation barrier and is energetically favorable. Also, intermediate **VII** appears to be another 3-coordinated intermediate likely to occur during the global reaction.

Finding the Second Intermediate. Once the first intermediate was identified, we continued exploring the reaction mechanism by assessing the existence of a second intermediate. First, we probed the possibility of a 2-coordinated intermediate occurring after intermediate **V** [reactions L and M, Table 2, Figure S3 (Supporting Information)]. Consistent with reactions E and F, 2-coordinated intermediates **I** and **II** are not stable species in the potential energy profile, and both are formed with large kinetic barriers (Table 3). Next, we assessed the formation of a tetrahedral intermediate after intermediate **V** [reaction N, Table 2, Figure S4 (Supporting Information)]. This reaction occurs with $E_a \approx 8$ kcal/mol and yields a metastable intermediate **IX** (Table 3), supporting our previous conclusions based on reaction K.

Once 2- and 4-coordinated species were ruled out from the reaction mechanism based on our findings, we investigated the potential energy profiles of binding Cys2_W and deCOORDinating either Cys1_A or Cys2_A to form 3-coordinated intermediates **VII** and **VIII** from intermediate **V** (reactions O and P, Table 2, Figure 5). Reaction O proceeds with high E_a and the formation of one intermediate that is similar to the product of this reaction (intermediate **VIII**). On the other hand, reaction P proceeds in a concerted fashion, yielding the stable intermediate **VII** after overcoming an activation barrier of 9.5 kcal/mol (Table 3). Consistent with our previous results based on reactions E–H,

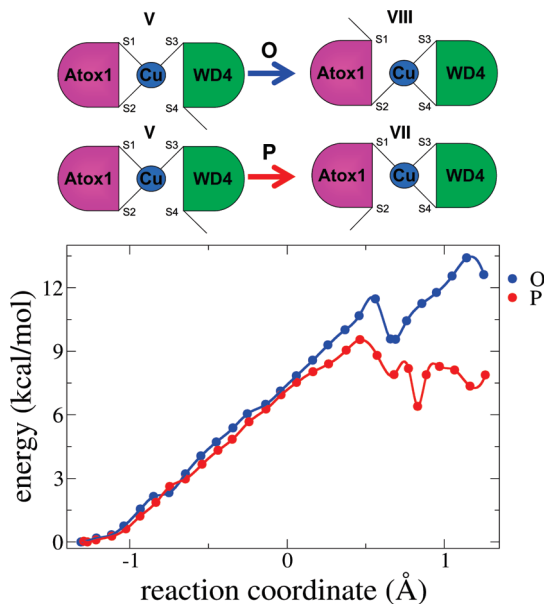


Figure 5. Potential energy profile (kcal/mol) along the corresponding reaction coordinate (Å) defined in Table 2 for reactions O (blue) and P (red). A schematic of the species (defined in Table 1) involved in each reaction is also shown.

intermediate **V** is more stable than intermediate **VII** by ~ 6 kcal/mol, and it is kinetically more feasible to form **VII** than **VIII**.

We also probed the possibility of a concerted reaction toward the reaction product from intermediate **V** [reaction Q, Table 2, Figure S5 (Supporting Information)]. As expected, this reaction does not occur in a concerted fashion, but instead proceeds with the existence of two **VII**-like intermediates that are similar in energy, after overcoming an activation barrier of ~ 10 kcal/mol (Table 3). All together, this group of reactions supports the existence of the 3-coordinated species **VII** as the second intermediate of the global Cu-transfer reaction from Atox1 to WD4. These results again emphasize that 3-coordinated species are more stable than 2- or 4-coordinated species.

We finally studied the last step of the reaction, in which, starting from intermediate **VII**, Cys1_A is decoordinated from Cu(I) [reaction R, Table 2, Figure 6]. This reaction occurs with $E_a \approx 8$ kcal/mol to yield the product of the reaction, which is ~ 6 kcal/mol less stable than the second intermediate **VII** (Table 3).

Overview of the Reaction Mechanism. Based on all of the above reactions, we can suggest the most probable reaction mechanism of Cu(I) transfer from holo-Atox1 to apo-WD4 (Figure 7). The proposed reaction involves the two 3-coordinated intermediates **V** and **VII**, in which the Cys1 residues of both Atox1 and WD4 are always coordinated to the Cu(I) ion. Table 4 lists relevant geometrical parameters of the reactant, the two intermediates, and the product of the reaction. In all cases, the Cu center is surrounded by three water molecules that form hydrogen bonds with Cys1_A, Cys1_W, and Atox1's Thr11 (see Figure 1 for the reactant). Neither 2- nor 4-coordinated species appear to be intermediates of this reaction. Our results agree with mutagenesis and NMR experiments on two similar Cu chaperone–Cu–MBD adducts in which only three of the four functional Cys residues were required for adduct formation.^{17,43} These NMR results suggested that the Cys1 residues of both the metallochaperone and target domain were strictly required for adduct formation,^{17,43} which completely validates our identification of intermediates **V** and **VII** as the two intermediates of the Cu(I)-transfer reaction. Also, the intermediates **V**

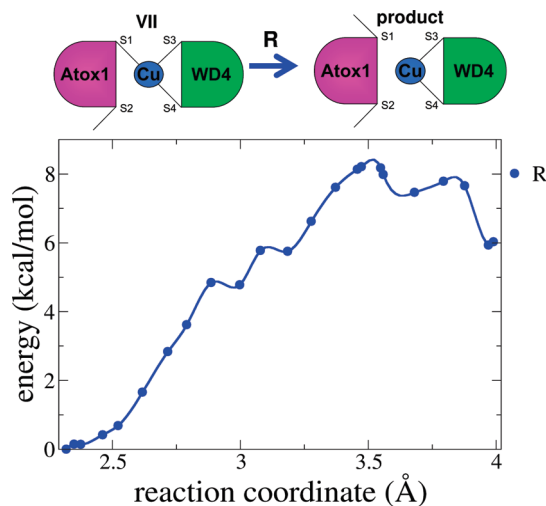


Figure 6. Potential energy profile (kcal/mol) along the corresponding reaction coordinate (Å) defined in Table 2 for reaction R. A schematic of the species (defined in Table 1) involved in the reaction is also shown.

and **VII** in our proposed reaction mechanism agree with the holo-Atox1 homodimer crystal structure, which suggested Cys1 as the first Cys to bind Cu(I) during Cu(I) transfer.¹⁹ Binding of Cys1_W as the first step of the Cu(I)-transfer reaction was not unexpected, because the first Cys residue is located in a surface-exposed loop and is always more exposed than the second Cys residue in this family of proteins,⁴⁴ which facilitates initial formation of the ternary complex.

Our proposed reaction mechanism was further validated by performing a final calculation in which the reaction coordinate was defined to go from the reactant all the way to the product [reaction S, Table 2, Figure S6 (Supporting Information)]. In this calculation, we can observe how the global reaction occurs, step by step, with sequential formation of the two intermediates **V** and **VII**, confirming all of our above predictions that are based on assessing individual steps. Moreover, upon inspection of reaction S, we note that the product of the reaction is less stable than the reactant.

The first step of the overall reaction (reaction A) proceeds without a kinetic barrier to form the first intermediate **V**, which is the most stable species of all (Figure 7). This result is in agreement with the observation of a stable Cu-dependent heterocomplex that Atox1 and WD4 form *in vitro*⁴⁵ and with the ability to detect a similar Atox1–MBD Cu-dependent adduct by NMR spectroscopy.¹⁷ After this initial step, the system has to overcome the rate-limiting step, which is formation of the second intermediate **VII** (reaction P), to finally form the product (reaction R). The overall reaction A–P–R (Figure 7) has a relatively low activation barrier, 9.5 kcal/mol, which suggests that the overall reaction is kinetically feasible. However, our results suggest that this reaction is not favored energetically, with an overall ΔE value of 7.7 kcal/mol (Figure 7). In the absence of a favorable thermodynamic gradient, a low activation barrier can still allow for rapid Cu(I) transfer from the metallochaperone to the target domain if this process is coupled to subsequent Cu(I) translocation into the Golgi lumen and ATP hydrolysis, as previously suggested.⁴⁶ On the other hand, it is tempting to speculate that, in the absence of a driving force (i.e., ATP hydrolysis), formation of the Cu(I)-bridged heterocomplex (species **V**) might be favored with respect to Cu(I) transfer.⁴⁵ However, we note that our QM/MM calculations do not take into account entropic effects, which will likely drive separation of the heterocomplex into individual species.

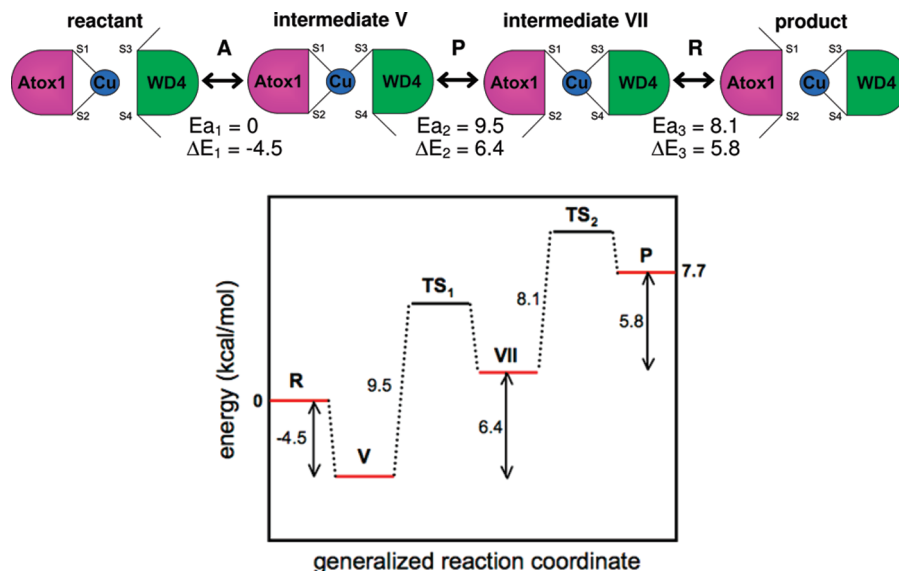


Figure 7. Top: Proposed reaction mechanism for the Cu-transfer reaction, showing a schematic of the Cu-center geometry of the reactant, two intermediates, and the product (as defined in Table 1). The name of the reaction step, the activation energy (E_a , kcal/mol), and the difference in potential energy (ΔE , kcal/mol) are included for each step. Bottom: Schematic of the potential energy (kcal/mol) as a function of the generalized reaction coordinate, showing the relative energies of the reactant (R), intermediates V and VII, and product (P), as well as the two transition states (TS₁ and TS₂).

TABLE 4: Relevant Distances (in Å) and Angles (in Degrees) from the Four Species of the Cu-Transfer Mechanism: Reactant, Product, and Intermediates V and VII^a

	reactant	intermediate V	intermediate VII	product
S1–Cu	2.18	2.29	2.35	3.97
S2–Cu	2.19	2.33	3.26	3.70
S3–Cu	3.54	2.37	2.32	2.16
S4–Cu	3.77	3.60	2.43	2.15
S1–Cu–S2	158.4	134.8	101.9	79.7
S2–Cu–S4	101.6	101.6	106.8	104.9
S4–Cu–S3	70.5	77.2	106.7	158.2
S3–Cu–S1	90.8	104.5	109.3	83.5
T11 _A (OG1)–Cu	3.61	3.49	4.34	4.71
T11 _A (OG1)–S3	3.94	3.75	3.83	3.78
T13 _W (OG1)–Cu	6.10	6.27	5.57	6.02
T13 _W (OG1)–S1	4.91	4.97	4.89	4.84
K60 _A (NZ)–Cu	3.79	3.75	3.51	3.17
K60 _A (NZ)–S2	3.13	3.09	3.05	3.06
K60 _A (NZ)–S4	2.96	2.96	3.01	3.08

^a S1 and S2, Atox1's Cys1(SG) and Cys2(SG), respectively; S3 and S4, WD4's Cys1(SG) and Cys2(SG), respectively; A, Atox1; W, WD4.

To explore the effect of Cys protonation in our proposed reaction mechanism of Cu(I) transfer from Atox1 to WD4, we repeated some of the key reactions [A', B' and R', Table 2, Figures S7–S9 (Supporting Information); compare reaction B' with C] with the Cys residues that were free at both the beginning and end of the calculation protonated (for this reason, reactions O and P could not be performed). These results are in agreement with our previous findings (Table 3) and also suggest that our proposed reaction pathway, shown in Figure 7, and our proposed reaction intermediates are independent of whether the Cys residues that are not coordinating the Cu(I) atom are protonated or not. This further suggests that deprotonation/protonation of those Cys residues could occur before or after Cu(I) binding to the other Cys residues.

Because our computed overall Cu-transfer reaction is endothermic, we searched for molecular determinants that could account for the difference in energy between the reactant and product. Close to the active sites, the most important difference

between Atox1 and WD4 is the presence of Lys60 in Atox1, which is a Phe residue in WD4. This Lys residue is believed to stabilize the Cu-bound state by neutralizing the overall negative charge of the Cu(I)–Cys₂ center. Initially, we thought that the presence of this Lys residue in Atox1 would account for the lower energy of the reactant heterocomplex (as compared to that of the product heterocomplex). However, inspection of the active sites of the QM/MM-optimized structures of the reactant and product reveals that the position of Lys60 is such that it is close to both active sites (Table 4), being able to stabilize both reactant and product states to the same extent. On the other hand, although both proteins contain a Thr residue in position X₁ of the MX₁CX₂X₃C motif, Thr is only close to the Cu(I) center in Atox1 (Thr11), whereas in WD4 it is facing the opposite side (Thr13) (Table 4). In the reactant, Atox1's Thr11 is close to Cu(I), stabilizing in this way Atox1's Cu-bound state. Instead, this same residue is farther from Cu(I) in the product, which might account, in part, for the reduced stabilization of WD4's Cu-bound state. The distance of Atox1's Thr11 to Cu(I) correlates with the relative energy in all species: reactant, intermediates X and XII, and product (Table 4). We have recently shown that both Thr11 and Lys60 in Atox1 are necessary to ensure optimal Cu transfer to WD4 in vitro.⁴⁵

Dynamics of Interactions in Reactant and Product Heterocomplexes. To gain insight into structural and dynamic differences between the reactant and product, we performed MD simulations of the reactant [i.e., Cu(I) coordinated to Atox1's Cys] and product [i.e., Cu(I) coordinated to WD4's Cys] heterocomplexes. Although both heterocomplexes are stable during the ~120-ns MD runs as indicated by the backbone rmsd time evolution plot (Figure 8A), fluctuations are greater when Cu(I) is bound to WD4 (Figure 8B). Residues that define the Atox1–WD4 interface, including Atox1's Cu loop, helix α 1, and α 2– β 4 loop and WD4's Cu loop, helices α 1 and α 2, and α 2– β 4 loop, are more flexible in the product. This agrees with previous MD simulations on the individual proteins, which suggest that, whereas Atox1's flexibility is reduced upon Cu(I) binding,²² WD4 retains its flexibility even when bound to Cu(I).²¹

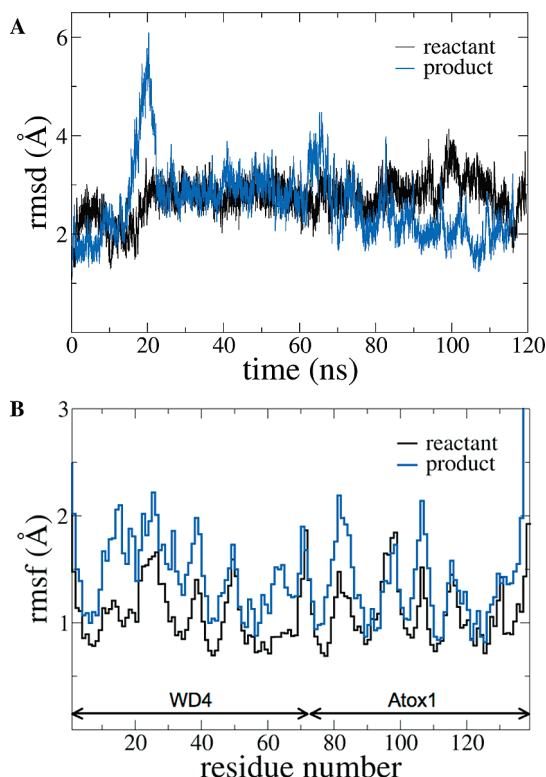


Figure 8. (A) rmsd (in Å, with respect to the first structure) of backbone heavy atoms as a function of the simulation time (ns) for the reactant (black) and product (blue) heterocomplexes. (B) Average fluctuations (rmsf in Å) of backbone heavy atoms per residue (for the last 50 ns of MD simulations) for the reactant (black) and product (blue) heterocomplexes. Reactant, Cu(I) coordinated to Atox1's Cys; product, Cu(I) coordinated to WD4's Cys.

TABLE 5: Free Energy (ΔG) of Reactant (holo-Atox1–WD4) and Product (Atox1–holo-WD4) Hetero-complex Formation, Including Its Different Energetic Contributions: Intermolecular van der Waals Interactions (vdW), Change in Nonpolar Solvation Energy (Cavity), Intermolecular Coulomb Interactions (Electrostatic), And Change in Reaction Field Energy (Field)^a

	ΔG	vdW	cavity	electrostatic	field
reactant	-9.2 ± 0.7	-50 ± 5	-9.1 ± 0.6	-137 ± 21	136 ± 19
product	-7.1 ± 0.8	-35 ± 7	-7 ± 1	-205 ± 17	206 ± 16

^a All energy values are in kcal/mol; errors correspond to the standard deviation.

To quantify the strength of the protein–protein interactions and complex stability, we estimated the free energy (ΔG) of heterocomplex formation (Table 5). Interestingly, the reactant heterocomplex is ~ 2 kcal/mol more stable than the product, which is consistent with the observed endothermic nature of the overall Cu(I)-transfer reaction. Although Coulombic interactions increase in the product compared to the reactant, the change in reaction field energy increases even more, to the point that the combined contribution is slightly favorable for the reactant but slightly unfavorable for the product. On the other hand, contributions from van der Waals interactions and the change in nonpolar solvation energy are much smaller in the product, indicating less compactness of this complex and accounting for the overall stability difference. It appears that the less favorable ΔG value of the product arises in part from an increase in backbone fluctuations of holo-WD4 in this heterocomplex (Figure 8B), as discussed above. In the reactant, the reduced flexibility of holo-Atox1 contributes to maintain a stable

intermolecular network between conserved residues, which keep Atox1's and WD4's active sites in close contact.²¹ In the product, however, holo-WD4's enhanced flexibility “pushes” the active sites farther away, weakening the interacting network. It is tempting to speculate that the increase in flexibility of holo-WD4 is a way to ensure that the complex will dissociate once Cu(I) is transferred to WD4, contributing in this way to promote directional Cu(I) transfer into the Golgi lumen in vivo.

Recent MD simulations of holo-Atox1 Thr11Ala and Lys60Ala point variants in complex with WD4 (reactant heterocomplex) suggest that Thr11 and Lys60 in Atox1 are important for correct positioning of the two active sites and adduct stability.⁴⁵ Because the product heterocomplex appears to be less stable than the reactant, we predict that mutations of residues 11 and 60 in Atox1 will result in stronger effects in the product.

Conclusions

We have used a QM/MM approach to investigate all possible reaction schemes for how Cu(I) is transferred from the two Cys residues in the human Cu chaperone Atox1 to the corresponding two Cys residues in one of the MBDs of the target Wilson disease protein, WD4. In agreement with previously published experiments,^{17,43} our results suggest that 3-coordinate Cu intermediates are more stable than 2- or 4-coordinated intermediates. Furthermore, we propose that two intermediates exist on the reaction pathway from Cu–Atox1 and apo-WD4 to apo-Atox1 and Cu–WD4 (species V and VII, Table 1). First, Cys1 of WD4 coordinates Cu(I) together with the two Cys residues from Atox1 (V). The next step, which is rate-limiting for the overall reaction, involves a concerted switch to another 3-coordinated species that involves Cys1 of Atox1 and both of the Cys residues in WD4 (VII). Our findings suggest that the overall reaction, although kinetically accessible, is endothermic. Although entropic effects might contribute to heterocomplex separation, this suggests that other factors (e.g., ATP hydrolysis) must contribute to ensure that Cu(I) transfer is directional in vivo. The reaction mechanism suggested here might be also extended to the other WDs that receive Cu(I) from Atox1 (for example, WD2) or to the MBDs of the Menkes ATPase. Because Cu is an essential trace metal in humans, several diseases have been linked to Cu mismetabolism/accumulation,^{47,48} and the Wilson disease protein has been proposed to contribute to cell resistance to the cancer drug cisplatin.^{49,50} It is of utmost importance to elucidate mechanisms of metal transfer between these proteins. Computational methods such as the QM/MM calculations employed here provide molecular details not easily accessible by in vitro experiments.

Abbreviations

Cu, copper; MBD, metal-binding domain; WD, MBD of Wilson disease protein; QM/MM, quantum mechanics/molecular mechanics; MD, molecular dynamics; ΔG , free energy; E_a , activation energy.

Acknowledgment. This work was supported by the Shared University Grid at Rice (NSF Grant EIA-0216467) and by a partnership between Rice University, Sun Microsystems, and Sigma Solutions, Inc. D.E. acknowledges funds from CONICET PIP 1207. P.W.S. acknowledges funds from the Kempe and Wallenberg foundations and the Swedish Research Council.

Supporting Information Available: Potential energy profiles along the corresponding reaction coordinates defined in Table 2 for reactions B–D, I and J, L and M, N, Q, S, A', B',

and R' (Figures S1–S9, respectively). Schematics of the species involved in the reactions are also included in each figure. This material is available free of charge via the Internet at <http://pubs.acs.org>.

References and Notes

- Bertinato, J.; L'Abbe, M. R. *J. Nutr. Biochem.* **2004**, *15*, 316.
- Lutsenko, S.; Barnes, N. L.; Bartee, M. Y.; Dmitriev, O. Y. *Physiological Reviews* **2007**, *87*, 1011.
- Pufahl, R. A.; Singer, C. P.; Peariso, K. L.; Lin, S. J.; Schmidt, P. J.; Fahrni, C. J.; Culotta, V. C.; Penner-Hahn, J. E.; O'Halloran, T. V. *Science* **1997**, *278*, 853.
- Klomp, L. W.; Lin, S. J.; Yuan, D. S.; Klausner, R. D.; Culotta, V. C.; Gitlin, J. D. *J. Biol. Chem.* **1997**, *272*, 9221.
- Hung, I. H.; Casareno, R. L.; Labesse, G.; Mathews, F. S.; Gitlin, J. D. *J. Biol. Chem.* **1998**, *273*, 1749.
- Larin, D.; Mekios, C.; Das, K.; Ross, B.; Yang, A. S.; Gilliam, T. C. *J. Biol. Chem.* **1999**, *274*, 28497.
- Strausak, D.; Howie, M. K.; Firth, S. D.; Schlicksupp, A.; Pipkorn, R.; Multhaup, G.; Mercer, J. F. *J. Biol. Chem.* **2003**, *278*, 20821.
- van Dongen, E. M.; Klomp, L. W.; Merks, M. *Biochem. Biophys. Res. Commun.* **2004**, *323*, 789.
- Walker, J. M.; Huster, D.; Ralle, M.; Morgan, C. T.; Blackburn, N. J.; Lutsenko, S. *J. Biol. Chem.* **2004**, *279*, 15376.
- Achila, D.; Banci, L.; Bertini, I.; Bunce, J.; Ciofi-Baffoni, S.; Huffman, D. L. *Proc. Natl. Acad. Sci. U.S.A.* **2006**, *103*, 5729.
- Banci, L.; Bertini, I.; Cantini, F.; Rosenzweig, A. C.; Yatsunyk, L. A. *Biochemistry* **2008**, *47*, 7423.
- Banci, L.; Bertini, I.; Cantini, F.; Massagni, C.; Migliardi, M.; Rosato, A. *J. Biol. Chem.* **2009**, *284*, 9354.
- DiDonato, M.; Narindrasorasak, S.; Forbes, J. R.; Cox, D. W.; Sarkar, B. *J. Biol. Chem.* **1997**, *272*, 33279.
- Lutsenko, S.; Petrukhin, K.; Cooper, M. J.; Gilliam, C. T.; Kaplan, J. H. *J. Biol. Chem.* **1997**, *272*, 18939.
- Wernimont, A. K.; Huffman, D. L.; Lamb, A. L.; O'Halloran, T. V.; Rosenzweig, A. C. *Nat. Struct. Biol.* **2000**, *7*, 766.
- Banci, L.; Bertini, I.; Cantini, F.; Felli, I. C.; Gonnelli, L.; Hadjiliadis, N.; Pierattelli, R.; Rosato, A.; Voulgaris, P. *Nat. Chem. Biol.* **2006**, *2*, 367.
- Banci, L.; Bertini, I.; Calderone, V.; Della-Malva, N.; Felli, I. C.; Neri, S.; Pavelkova, A.; Rosato, A. *Biochem. J.* **2009**, *422*, 37.
- Benitez, J. J.; Keller, A. M.; Ochieng, P.; Yatsunyk, L. A.; Huffman, D. L.; Rosenzweig, A. C.; Chen, P. *J. Am. Chem. Soc.* **2008**, *130*, 2446.
- Wernimont, A. K.; Huffman, D. L.; Lamb, A. L.; O'Halloran, T. V.; Rosenzweig, A. C. *Nat. Struct. Biol.* **2000**, *7*, 766.
- Holt, B. T.; Merz, K. M., Jr. *Biochemistry* **2007**, *46*, 8816.
- Rodriguez-Granillo, A.; Crespo, A.; Wittung-Stafshede, P. *Biochemistry* **2009**, *48*, 5849.
- Rodriguez-Granillo, A.; Wittung-Stafshede, P. *J. Phys. Chem. B* **2008**, *112*, 4583.
- Eswar, N.; Webb, B.; Marti-Renom, M. A.; Madhusudhan, M. S.; Eramian, D.; Shen, M. Y.; Pieper, U.; Sali, A. *Comparative Protein Structure Modeling Using MODELLER*. In *Current Protocols in Protein Science*; John Wiley & Sons, Inc.: New York, 2007; Chapter 2, Unit 2.9.
- Banci, L.; Bertini, I.; Cantini, F.; Massagni, C.; Migliardi, M.; Rosato, A. *J. Biol. Chem.* **2009**, *284*, 9354.
- Banci, L.; Bertini, I.; Cantini, F.; Della-Malva, N.; Migliardi, M.; Rosato, A. *J. Biol. Chem.* **2007**, *282*, 23140.
- Cornell, W. D.; Cieplak, P.; Bayly, C. I.; Gould, I. R.; Merz, K. M.; Ferguson, D. M.; Spellmeyer, D. C.; Fox, T.; Caldwell, J. W.; Kollman, P. A. *J. Am. Chem. Soc.* **1995**, *117*, 5179.
- Pearlman, D. A.; Case, D. A.; Caldwell, J. W.; Ross, W. S.; Cheatham III, T. E.; DeBolt, S.; Ferguson, D.; Seibel, G.; Kollman, P. *Comput. Phys. Commun.* **1995**, *91*, 1.
- Case, D. A.; Cheatham, T. E., 3rd; Darden, T.; Gohlke, H.; Luo, R.; Merz, K. M., Jr.; Onufriev, A.; Simmerling, C.; Wang, B.; Woods, R. J. *J. Comput. Chem.* **2005**, *26*, 1668.
- Case, D. A.; Darden, T. A.; Cheatham, T. E., 3rd; Simmerling, C. L.; Wang, J.; Duke, R. E.; Luo, R.; Merz, K. M.; Pearlman, D. A.; Crowley, M.; Walker, R. C.; Zhang, W.; Wang, B.; Hayik, S.; Roitberg, A.; Seabra, G.; Wong, K. F.; Paesani, F.; Wu, X.; Brozell, S.; Tsui, V.; Gohlke, H.; Yang, L.; Tan, C.; Mongan, J.; Hornak, V.; Cui, G.; Beroza, P.; Mathews, D. H.; Schafmeister, C.; Ross, W. S.; Kollman, P. A. *Amber 9*; University of California: San Francisco, 2006.
- Jorgensen, W. L.; Chandrasekhar, J.; Madura, J.; Impey, R. W.; Klein, M. L. *J. Chem. Phys.* **1983**, *79*, 926.
- Hornak, V.; Abel, R.; Okur, A.; Strockbine, B.; Roitberg, A.; Simmerling, C. *Proteins* **2006**, *65*, 712.
- Berendsen, H. J.; Postma, J. P.; van Gunsteren, W. F.; Di Nola, A.; Haak, J. R. *J. Chem. Phys.* **1984**, *81*, 3684.
- Ryckaert, J. P.; Ciccotti, G.; Berendsen, H. J. C. *J. Comput. Phys.* **1977**, *23*, 327.
- Naim, M.; Bhat, S.; Rankin, K. N.; Dennis, S.; Chowdhury, S. F.; Siddiqi, I.; Drabik, P.; Sulea, T.; Bayly, C. I.; Jakalian, A.; Purisima, E. O. *J. Chem. Inf. Model.* **2007**, *47*, 122.
- Cui, Q.; Sulea, T.; Schrag, J. D.; Munger, C.; Hung, M. N.; Naim, M.; Cygler, M.; Purisima, E. O. *J. Mol. Biol.* **2008**, *379*, 787.
- Chen, W.; Chang, C. E.; Gilson, M. K. *Biophys. J.* **2004**, *87*, 3035.
- Crespo, A.; Scherlis, D. A.; Marti, M. A.; Ordejón, P.; Roitberg, A. E.; Estrin, D. A. *J. Phys. Chem. B* **2003**, *107*, 13728.
- Soler, J. M.; Artacho, E.; Gale, J. D.; Garcia, A.; Junquera, J.; Ordejón, P.; Sanchez-Portal, D. *J. Phys.: Condens. Matter* **2002**, *14*, 2745.
- Perdew, J. P.; Burke, K.; Ernzerhof, M. *Phys. Rev. Lett.* **1996**, *77*, 3865.
- Crespo, A.; Marti, M. A.; Roitberg, A. E.; Amzel, L. M.; Estrin, D. A. *J. Am. Chem. Soc.* **2006**, *128*, 12817.
- Eichinger, M.; Tavan, P.; Hutter, J.; Parrinello, M. *J. Chem. Phys.* **1999**, *110*, 10452.
- Wang, J.; Cieplak, P.; Kollman, P. A. *J. Comput. Chem.* **2000**, *21*, 1049.
- Banci, L.; Bertini, I.; Cantini, F.; Felli, I. C.; Gonnelli, L.; Hadjiliadis, N.; Pierattelli, R.; Rosato, A.; Voulgaris, P. *Nat. Chem. Biol.* **2006**, *2*, 367.
- Arnesano, F.; Banci, L.; Bertini, I.; Ciofi-Baffoni, S.; Molteni, E.; Huffman, D. L.; O'Halloran, T. V. *Genome Res.* **2002**, *12*, 255.
- Hussain, F.; Rodriguez-Granillo, A.; Wittung-Stafshede, P. *J. Am. Chem. Soc.* **2009**, *131*, 16371.
- Huffman, D. L.; O'Halloran, T. V. *J. Biol. Chem.* **2000**, *275*, 18611.
- Gitlin, J. D. *Gastroenterology* **2003**, *125*, 1868.
- Tao, T. Y.; Gitlin, J. D. *Hepatology* **2003**, *37*, 1241.
- Leonhardt, K.; Gebhardt, R.; Mossner, J.; Lutsenko, S.; Huster, D. *J. Biol. Chem.* **2009**, *284*, 7793.
- Dolgova, N. V.; Olson, D.; Lutsenko, S.; Dmitriev, O. Y. *Biochem. J.* **2009**, *419*, 51.

JP911208Z